Photoemission, soft x-ray absorption, and magnetic circular dichroism spectroscopy study of $Fe_{1-x}Cu_xCr_2S_4$ ($0.1 \leq x \leq 0.5$) spinel sulfides

2006 J. Phys.: Condens. Matter 18 7413

(http://iopscience.iop.org/0953-8984/18/31/033)

INSTITUTE OF PHYSICS PUBLISHING JOURNAL OF PHYSICS: CONDENSED MATTER

J. Phys.: Condens. Matter **18** (2006) 7413–7426 doi:10.1088/0953-8984/18/31/033

Photoemission, soft x-ray absorption, and magnetic circular dichroism spectroscopy study of $Fe_{1-x}Cu_xCr_2S_4$ ($0.1 \leqslant x \leqslant 0.5$) spinel sulfides

S W Han[1], J-S Kang[1,2], S S Lee[2], G Kim[2], S J Kim[3], C S Kim[3], J-Y Kim[4], H J Shin[4], K H Kim[5], J I Jeong[6], B-G Park[7], J-H Park[7] and B I Min[7]

[1] CSCMR, Seoul National University, Seoul 151-742, Korea
[2] Department of Physics, The Catholic University of Korea, Bucheon 420-743, Korea
[3] Department of Physics, Kookmin University, Seoul 136-702, Korea
[4] Pohang Accelerator Laboratory, POSTECH, Pohang 790-784, Korea
[5] Department of Physics and RINS, Gyeongsang National University, Jinju 660-701, Korea
[6] Research Institute of Industrial Science and Technology, Pohang 790-330, Korea
[7] Department of Physics, POSTECH, Pohang 790-784, Korea

E-mail: kangjs@catholic.ac.kr

Received 6 May 2006, in final form 11 June 2006
Published 21 July 2006
Online at stacks.iop.org/JPhysCM/18/7413

Abstract

The electronic and magnetic structures of $Fe_{1-x}Cu_xCr_2S_4$ ($0.1 \leqslant x \leqslant 0.5$) spinel sulfides have been investigated systematically by performing photoemission spectroscopy (PES), soft x-ray absorption spectroscopy (XAS), and soft x-ray magnetic circular dichroism (XMCD) measurements using synchrotron radiation. Cr and Cu ions are found to be nearly trivalent (Cr^{3+}) and monovalent (Cu^{+}), respectively, and their valence states do not change with x. The Fe 2p XAS spectra of $Fe_{1-x}Cu_xCr_2S_4$ are very similar to that of Fe metal, indicating that the Fe 3d electrons are strongly hybridized to other valence electrons. The Fe and Cr 2p XMCD spectra show that the magnetic moments of Cr ions and Fe ions are aligned antiparallel to each other and that both the Cr and Fe magnetic moments increase with increasing x. The valence-band PES study reveals that the Cr^{3+} ($t_{2g}^3 \downarrow$) 3d states are located at $\sim$1.5 eV below E_F. The occupied Fe 3d states consist of the broad $t_{2g}^3 \uparrow$ states, the $e_g^2 \uparrow$ states at $\sim$4 eV below E_F, and the $e_g \downarrow$ states very close to E_F. The filled Cu $3d^{10}$ states lie at $\sim$2.5 eV below E_F. This study suggests that the hybridized Fe $e_g \downarrow$ and S 3p states near E_F play an important role in determining the transport properties of $Fe_{1-x}Cu_xCr_2S_4$ for $x \leqslant 0.5$.

(Some figures in this article are in colour only in the electronic version)

1. Introduction

Spinel compounds of $Fe_{1-x}Cu_xCr_2S_4$ ($x = 0$, 0.5) exhibit a very large negative magnetoresistance (MR) effect, the size of which is as large as that of the giant magnetoresistance (GMR) in metallic multilayers [1, 2]. Upon cooling, the resistivity $\rho(T)$ shows a crossover from insulator to metal near the magnetic transition temperature T_C, and then back to the insulating feature far below T_C, that is, $d\rho/dT < 0$ for high and low temperatures ($T > T_C$ and $T \ll T_C$), and $d\rho/dT > 0$ in between. The temperature range showing the metallic feature is wider for $x = 0.5$ than for $x = 0$. The metal–insulator (M–I) crossover occurs together with the magnetic transition for $0.1 \leqslant x \leqslant 0.5$ [3]. With increasing x in $Fe_{1-x}Cu_xCr_2S_4$, T_C increases monotonically, whereas the room temperature resistivity and the MR decrease first and then increase to exhibit local minima near $x = 0.2$ and local maxima at $x = 0.5$ [4–7]. For $x > 0.5$, both the resistivity and the MR decrease monotonically. The ideal spinel structure of the ordered $Fe_{1-x}Cu_xCr_2S_4$ is formed by a close-packed face-centred cubic (fcc) array of sulfur (S) atoms with the metal atoms occupying the interstitial positions (see figure 1). Fe and Cu ions occupy the tetrahedral (T_d) sites and Cr ions occupy the octahedral (O_h) sites, surrounded by four and six S ions, respectively. There are two formula units in the primitive unit cell. It is considered that each of the Fe and Cr sublattices orders ferromagnetically, while the two sublattices are coupled antiferromagnetically to each other, resulting in the ferrimagnetic ground states [8].

It has been pointed out that the mechanisms of the M–I crossover transition and the magnetic transition in the spinel compounds are different from those in the colossal magnetoresistance (CMR) perovskite manganites [2]. The nominal valence state of $FeCr_2S_4$ is considered to be $Fe^{2+}Cr_2^{3+}S_4^{2-}$, and so there are no mixed-valent ions, such as Mn^{3+}–Mn^{4+} ions in perovskite manganites, which allow the simultaneous metallic conductivity and ferromagnetic ordering via the double-exchange (DE) interaction. Further, the Jahn–Teller effect in $Fe_{1-x}Cu_xCr_2S_4$ does not play an essential role, which is also different from perovskite manganites. In order to explain the physical properties of $Fe_{1-x}Cu_xCr_2S_4$ ($x > 0.5$), two competing models have been proposed, with different valence states of the constituent elements. For $CuCr_2S_4$, Lotgering and van Stapele [9] developed a model considering the monovalent Cu^+ ions. If the Cu ion is monovalent in $CuCr_2S_4$, the valence configuration of $Cu^+[Cr^{3+}Cr^{4+}]S_4^{2-}$ is expected, implying the formally mixed-valent Cr ions. The ferromagnetic metallic ground state of $CuCr_2S_4$ was attributed to the DE interaction between Cr^{3+} ($3d^3$) and Cr^{4+} ($3d^2$) ions. Then, assuming the monovalent Cu^+ ions over the whole concentration range in $Fe_{1-x}Cu_xCr_2S_4$, Lotgering *et al* [5] have proposed the valence configurations of $Fe_{1-x}Cu_xCr_2S_4$ such that $Fe_{1-2x}^{2+}Fe_x^{3+}Cu_x^+Cr_2^{3+}S_4^{2-}$ for ($x \leqslant 0.5$) and $Fe_{1-x}^{3+}Cu_x^+[Cr_{3-2x+\delta}^{3+}Cr_{2x-1-\delta}^{4+}]S_{4-\delta}^{2-}S_\delta^-$ for ($x > 0.5$). Here S^- represents a hole in the valence band. On the other hand, Goodenough [10] postulated divalent Cu^{2+} ions and trivalent Cr^{3+} ions for $x > 0.5$.

Various experiments give different results on the valence states of the constituent elements. Cu 2p core-level x-ray photoemission spectroscopy (XPS) [11–13] and x-ray emission spectroscopy (XES) [11, 13] for CuM_2X_4 (M = V, Cr, Rh, Ir; X = S, Se) suggested that Cu ions are monovalent (Cu^+). Neutron diffraction data for $CuCr_2X_4$ (X = Se, Te) [14] were interpreted to represent monovalent Cu^+ ions and trivalent Cr^{3+} ions. Cr 2p and Cu 2p core-level XPS measurements [15] for $x = 0$ and $x = 0.5$ in $Fe_{1-x}Cu_xCr_2S_4$ showed that Cr ions are trivalent (Cr^{3+}: $3d^3$), and that Cu ions for $x = 0.5$ are likely to be monovalent (Cu^+: $3d^{10}$). Valence-band photoemission spectroscopy (PES) [16] for $Fe_{0.5}Cu_{0.5}Cr_2S_4$ showed that Cu ions are monovalent (Cu^+: $3d^{10}$). On the other hand, the experimental results of NMR [17], and magnetic properties [18] were interpreted in terms of divalent Cu^{2+} ($3d^9$) ions. Recent

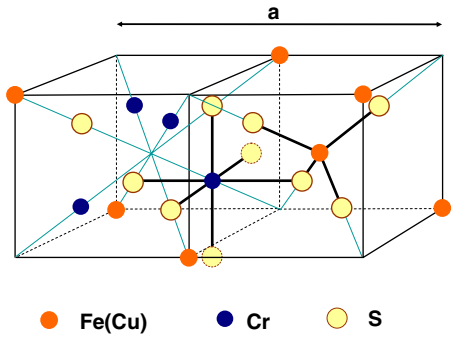

Figure 1. Spinel structure of $Fe(Cu)Cr_2S_4$. Fe(Cu) ions are at the tetrahedral (T_d) sites, and Cr ions are at the octahedral (O_h) sites.

Mössbauer spectroscopy measurements [3, 19] for $Fe_{1-x}Cu_xCr_2S_4$ revealed that Fe ions are divalent (Fe^{2+}) for $x \leqslant 0.1$, but trivalent (Fe^{3+}) for $x \geqslant 0.3$. In spite of extensive studies on the valence states of transition-metal elements in spinel systems, this issue has not been settled yet.

Therefore, it is necessary to perform the element-specific experiment that provides the direct information on the electronic and magnetic structure of $Fe_{1-x}Cu_xCr_2S_4$ ($0 \leqslant x \leqslant 1$). PES is an important experimental tool for studying the electronic structures of solids [20]. Soft x-ray absorption spectroscopy (XAS) is ideal for studying the valence states of T ions in solids [21, 22]. Soft x-ray magnetic circular dichroism (XMCD) is a powerful tool for studying the element-specific local magnetic moments of both spin (m_s) and orbital (m_l) components [23, 24]. In both XAS and XMCD, photons at specific characteristic energies are absorbed to produce the transition of a core electron to an empty state above the Fermi level, which is governed by the dipole selection rules. T 2p XAS and XMCD spectra of transition-metal oxides often show the multiplet structures, which arise from the electron–electron interaction within the T atom, and the crystal field splitting. The line shapes of XAS and XMCD spectra are strongly dependent on the occupied 3d electron configurations, the crystal field, and the hybridization of 3d electrons to other valence electrons. Thus the peak positions and the line shape of the T 2p XAS spectrum depend on the local electronic structure of the T ion, providing the information about the valence state and the ground state symmetry of the T ion. The magnitudes of m_s and m_l can be estimated quantitatively by applying the sum rules to the measured XMCD spectrum [24].

We have carried out PES, soft x-ray XAS, and XMCD experiments for polycrystalline samples of $Fe_{1-x}Cu_xCr_2S_4$ ($0.1 \leqslant x \leqslant 0.5$). From the measured T 2p XAS spectra (T = Fe, Cr, Cu), the valence states of Fe, Cr, and Cu ions in $Fe_{1-x}Cu_xCr_2S_4$ have been determined. From the measured valence-band PES spectra, we have determined the partial spectral weight (PSW) distributions of the different orbital states, such as Cr 3d, Fe 3d, Cu 3d, and S 3p states, and provided the schematic partial densities of states (PDOSs) in $Fe_{1-x}Cu_xCr_2S_4$. From the measured Cr 2p and Fe 2p XMCD spectra, the polarities and the individual magnetic moments of the Cr and Fe ions have been investigated. Based on these experiments, we will discuss the role of the electronic and magnetic structures of $Fe_{1-x}Cu_xCr_2S_4$ in determining their physical properties.

2. Experimental details

The polycrystalline samples were prepared by the standard solid-state reaction method [3]. Valence-band PES and XAS measurements were performed at both the 8A1 and 2A1 undulator

beamlines of the Pohang Accelerator Laboratory (PAL). The base pressure of both chambers was better than 4×10^{-10} Torr. The Fermi level E_F and the overall instrumental resolution (FWHM: full width at half maximum) of the system were determined from the valence-band spectrum of a scraped Pd metal in electrical contact with samples. The XAS spectra were obtained by employing the total electron yield method. All the spectra were normalized to the incident photon flux. Samples were cleaned *in situ* by repeated scraping with a diamond file. The cleanliness of the sample surfaces was monitored by the disappearance of the oxygen-related features in the Fe 2p and Cu 2p XAS spectra [25] and in the survey PES spectra after scraping. The $x = 0.1$ sample needed much caution because it easily became oxidized even after scraping in ultra-high vacuum. On the other hand, the $x = 0.5$ sample was more stable after scraping. We made scanning photoelectron microscopy (SPEM) measurements for some of the $Fe_{1-x}Cu_xCr_2S_4$ samples, which is known to be a powerful tool for studying the chemical distribution of specific elements in the sub-μm scale [26]. The measured SPEM images show that Cu ions were substituted for Fe ions homogeneously at least on the μm scale.

All the room-temperature (RT) measurements were performed at the 8A1 beamline. At the 8A1 beamline, the FWHM for PES was set at 100–400 meV between $h\nu = 130$ and 700 eV, and the FWHM for XAS was set at ~100 meV at $h\nu \approx 600$ eV. At the 2A1 beamline, the FWHM for PES was set at ~300 meV at $h\nu \sim 600$ eV, and the total resolution for XAS was ~150 meV at the Cr and Fe 2p edges and ~300 meV at the Cu 2p edge. All the low-temperature (LT) measurements and XMCD measurements were performed at the 2A1 beamline ($20\ \text{K} \leqslant T \leqslant 150\ \text{K}$). The 2A1 beamline is an elliptically polarized undulator, from which circularly polarized light was obtained with the degree of circular polarization of >90%. The XMCD spectra were taken for a fixed helicity of light by reversing the applied magnetic field (0.5 T) at each $h\nu$. In order to minimize the artificial effects caused by the decreasing photon flux with time, the direction of the applied magnetic field was reversed at each data point in the XMCD data acquisition. The total resolution for XMCD measurement was about 150 meV at the Cr and Fe 2p edges.

3. Results and discussion

3.1. T 2p XAS (T = Fe, Cu, Cr)

Figure 2 compares the Cr 2p XAS spectra of $Fe_{1-x}Cu_xCr_2S_4$ ($x = 0.1$, 0.2, 0.3, 0.5) to those of reference Cr compounds, such as Cr_2O_3 (formally Cr^{3+}) [27], $CrO_2(1)$ (formally Cr^{4+}) [28], $CrO_2(2)$ (formally Cr^{4+}) [29], $CuCr_2S_4$ (having the same spinel structure) [30], and Cr metal [31]. The XAS spectrum for Cr metal corresponds to that for Fe/Cr multilayer films. The XAS spectrum for $CrO_2(1)$ seems to represent a mixture of Cr_2O_3 and CrO_2 phases because CrO_2 is metastable near the *surface* region [29, 32].

This figure shows that the Cr 2p XAS spectra of $Fe_{1-x}Cu_xCr_2S_4$ for different x are identical to each other, indicating that the valence states of Cr ions do not change with the substitution of Cu ions in $Fe_{1-x}Cu_xCr_2S_4$. Further, the Cr 2p XAS spectra of $Fe_{1-x}Cu_xCr_2S_4$ are qualitatively similar to that of Cr_2O_3, but very different from those of Cr metal and CrO_2. These observations indicate that Cr ions in $Fe_{1-x}Cu_xCr_2S_4$ are mainly trivalent (3+) with the t_{2g}^3 configuration for $0.1 \leqslant x \leqslant 0.5$. Finally, the multiplet structures in $Fe_{1-x}Cu_xCr_2S_4$ are not so sharp as in Cr_2O_3, reflecting that the character of the Cr–S bonding in $Fe_{1-x}Cu_xCr_2S_4$ is probably covalent bonding rather than ionic bonding as in Cr_2O_3. This is probably due to the weaker electronegativity of S ions than oxygen (O) ions. The general features of Cr 2p XAS spectra of $Fe_{1-x}Cu_xCr_2S_4$ are also similar to those of $CuCr_2S_4$. On the other hand, the XAS line shape of $CuCr_2S_4$ is less structured than those of $Fe_{1-x}Cu_xCr_2S_4$, suggesting that the

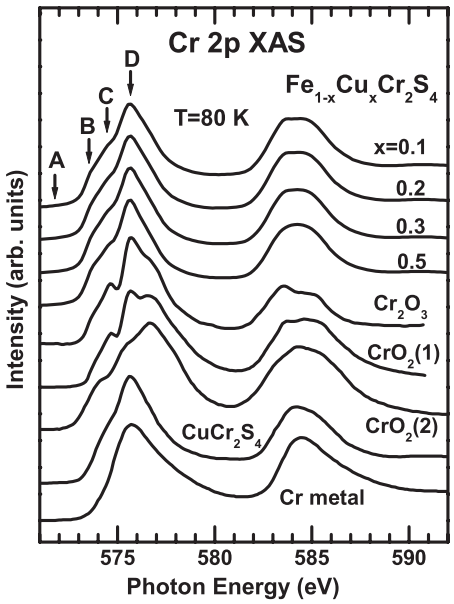

Figure 2. Comparison of the Cr 2p XAS spectra of $Fe_{1-x}Cu_xCr_2S_4$ to those of Cr_2O_3 (Cr^{3+}) [27], CrO_2(1) (Cr^{4+}) [28], CrO_2(2) (Cr^{4+}) [29], $CuCr_2S_4$ ($Cr^{3.5+}$) [30], and Cr metal [31]. Arrows A–D marked on the spectrum will be discussed in figure 5.

bonding character of Cr 3d electrons in $CuCr_2S_4$ is far from the simple ionic bonding. Then it is not easy to assign the formal valency for Cr ions in $CuCr_2S_4$ [30].

Figure 3 compares the Cu 2p XAS spectra of $Fe_{1-x}Cu_xCr_2S_4$ ($x = 0.1, 0.2, 0.3, 0.5$) to those of Cu_5FeS_4 [33], which is known to have the formally monovalent (+) Cu ions, and the formally divalent reference oxide CuO (2+) [34]. It is evident that the Cu 2p XAS spectra of $Fe_{1-x}Cu_xCr_2S_4$ ($x = 0.1, 0.2, 0.3, 0.5$) are essentially identical to each other, and that they are very similar to that of formally monovalent (Cu^+) Cu_5FeS_4, but quite different from that of CuO. The L_3 ($2p_{3/2}$) part for $Fe_{1-x}Cu_xCr_2S_4$ show three distinguishable peaks, one at $h\nu \approx 932$ eV (labelled as A), and the other two at $h\nu \approx 936$ eV (labelled as B) and $h\nu \approx 938$ eV (labelled as C). The same three-peak structures are repeated in the L_2 ($2p_{1/2}$) edge but more blurred due to the interaction with the L_3 continua. These features are typical of monovalent Cu^+ compounds with the $3d^{10}$ ground-state configuration. Note that the 2p XAS spectra of Cu^+ compounds are very different from those of Cu^{2+} compounds (see CuO at the bottom). Since the 3d band is full ($3d^{10}$) in the Cu^+ ground state, the strong peaks due to the transition from the Cu 2p core to the empty Cu 3d states are missing. That is, there are no strong peaks due to $2p^63d^n \rightarrow 2p^53d^{n+1}$ ($n \leqslant 9$) for the Cu^+ 2p XAS.

Therefore figure 3 provides evidence that Cu ions in $Fe_{1-x}Cu_xCr_2S_4$ are nearly monovalent ($3d^{10}$) for $x = 0.1, 0.2, 0.3, 0.5$. This finding is consistent with the Cu 2p core-level XPS study [35] of $Fe_{0.5}Cu_{0.5}Cr_2S_4$, the valence-band PES study [16] of $Fe_{0.5}Cu_{0.5}Cr_2S_4$, and the Cu 2p XAS study [30, 36] of $CuCr_2X_4$ (X = S, Se). We interpret the features in the Cu 2p XAS spectra of $Fe_{1-x}Cu_xCr_2S_4$ similarly as in Cu_5FeS_4 [33]. The hybridized ground state $|G\rangle$ of a monovalent Cu^+ ion is a linear combination of the three configurations, $|G\rangle = \alpha|3d^{10}\underline{L}4s^1\rangle + \beta|3d^{10}\rangle + \gamma|3d^94s^1\rangle$ ($\underline{L}$: a ligand hole), where the $|3d^{10}\underline{L}4s^1\rangle$ configuration is the lowest in energy, and $|\alpha|^2 \gg |\beta|^2, |\gamma|^2$. Strictly speaking, all the final states are also hybridized, consisting of a combination of all three configurations, such as $|2p^53d^{10}\underline{L}4s^2\rangle$,

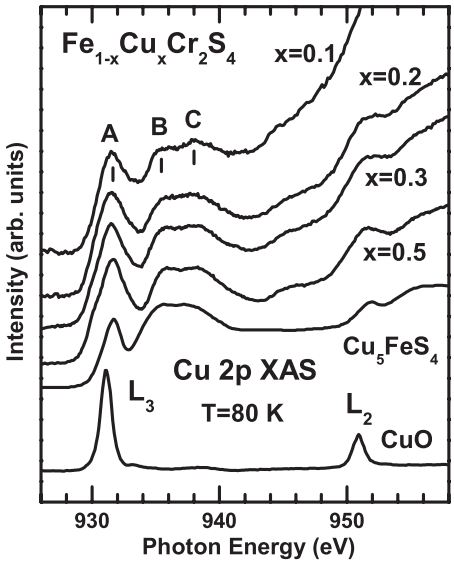

Figure 3. Comparison of the Cu 2p XAS spectra of $Fe_{1-x}Cu_xCr_2S_4$ ($x = 0.1$, 0.2, 0.3, 0.5) and Cu_5FeS_4 (Cu^+) [33], and CuO (Cu^{2+}) [34].

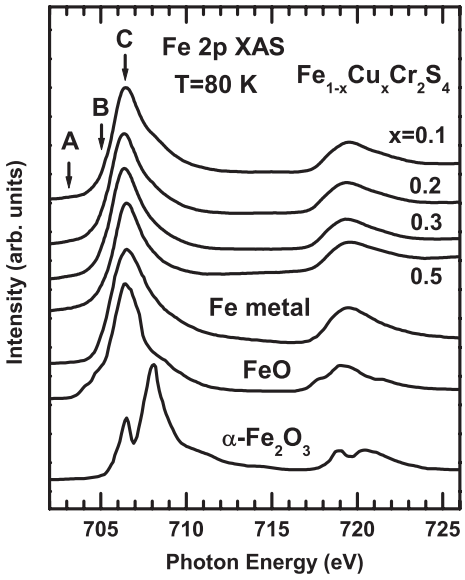

Figure 4. Comparison of the Fe 2p XAS spectra of $Fe_{1-x}Cu_xCr_2S_4$ to those of Fe metal [24] and FeO and α-Fe_2O_3 [25]. Arrows A, B, and C marked on the spectrum will be discussed in figure 5.

$|2p^53d^{10}4s^1\rangle$, $|2p^53d^94s^2\rangle$. Roughly speaking, however, the three peaks A, B, and C in the Cu 2p XAS can be assigned to the $|G\rangle \rightarrow |2p^53d^{10}\underline{L}4s^2\rangle$, $|G\rangle \rightarrow |2p^53d^{10}4s^1\rangle$, and $|G\rangle \rightarrow |2p^53d^94s^2\rangle$ transitions, respectively.

Figure 4 compares the Fe 2p XAS spectra of $Fe_{1-x}Cu_xCr_2S_4$ ($x = 0.1$, 0.2, 0.3, and 0.5) to those of Fe metal [24], FeO (formally Fe^{2+}) [25], and α-Fe_2O_3 (formally Fe^{3+}) [25], respectively. It is clearly shown that the Fe 2p XAS line shapes do not change for different Cu

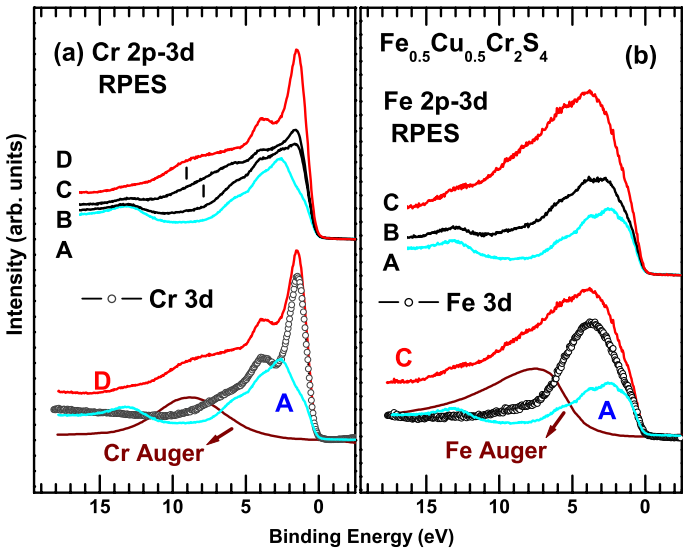

Figure 5. (a) The Cr 2p → 3d RPES and the extracted Cr 3d PSW for $Fe_{0.5}Cu_{0.5}Cr_2S_4$. Top: valence-band PES spectra, taken near the Cr $2p_{3/2}$ → 3d absorption edge, for $h\nu$ values marked in figure 2. Bottom: extraction procedure for the Cr 3d PSW. D (red) and A (blue) curves correspond to the on-resonance (D) and off-resonance (A) spectra, shown at the top. The curve at the bottom, marked with an arrow (brown) denotes the contribution of the Cr Auger emission underneath the on-resonance spectrum (D). Open circles denote the extracted Cr 3d PSW. (b) The Fe Cr 2p → 3d RPES and the extracted Fe 3d PSW for $Fe_{0.5}Cu_{0.5}Cr_2S_4$. All the notations in (b) are the same as in (a).

concentrations in $Fe_{1-x}Cu_xCr_2S_4$ ($0.1 \leqslant x \leqslant 0.5$), as if the valence states of Fe ions remain the same with the Cu substitution. This observation is rather unexpected, considering that the substituted Cu ions are monovalent (+) and that Mössbauer spectroscopy revealed trivalent Fe^{3+} ions for $x \geqslant 0.3$ in $Fe_{1-x}Cu_xCr_2S_4$ [3, 19]. We interpret the reason for this discrepancy as follows.

Note that the Fe 2p XAS spectra of $Fe_{1-x}Cu_xCr_2S_4$ are very similar to that of Fe metal, but quite different from those of FeO and Fe_2O_3, in that they do not have multiplet features in both $2p_{3/2}$ and $2p_{1/2}$ peaks. This observation indicates that the Fe 3d–S 3p bonding is very far from ionic bonding, and rather close to metallic-like bonding. In diluted magnetic semiconductors, it is well known that the impurity energy levels of Fe^{2+} ions are closer to the Fermi level than those of Cu^{2+} ions [37]. This feature is consistent with our observation for $Fe_{1-x}Cu_x^+Cr_2^{3+}S_4^{2-}$. Figures 2 and 3 indicate the trivalent states of Cr^{3+} ions and the monovalent states of Cu^+ ions. Considering the charge neutrality in semiconducting $Fe^{2+}Cr_2^{3+}S_4^{2-}$ and $Fe_{0.5}^{3+}Cu_{0.5}^+Cr_2^{3+}S_4^{2-}$, it is expected that there is a small increase in the Fe^{3+} (d^5) component with increasing x in $Fe_{1-x}Cu_xCr_2S_4$. Since Fe^{3+} (d^5) ions have one less d electron than Fe^{2+} (d^6) ions, this conclusion implies that the charge transfer occurs from Fe ions to Cu ions so as to increase the Fe^{3+} (d^5) component, with respect to the Fe^{2+} (d^6) component. On the other hand, the Fe 3d states are found to be strongly hybridized to the S 3p electrons in $Fe_{1-x}Cu_xCr_2S_4$ (see figure 4). Hence it is likely that the charge transfer occurs from the Fe–S hybridized states to the Cu states. We attribute the reason why the trend of the increasing valence states of Fe ions is not observed in the Fe 2p XAS spectra (see figure 4) to the large hybridization between Fe 3d and S 3p electrons. This point will be discussed further under the XMCD results. This finding makes a contrast to those for Cr 2p and Cu 2p XAS spectra, which indicate the covalent and/or ionic bonding for Cr and Cu 3d electrons, which will be also discussed further in figure 5.

3.2. Valence-band PES and PDOS

Figure 5 shows the valence-band RPES spectra of $Fe_{0.5}Cu_{0.5}Cr_2S_4$, taken near the Cr $2p_{3/2}$ and Fe $2p_{3/2}$ absorption edges and the extracted Cr and Fe 3d partial spectral weight (PSW) distributions. We have measured the valence-band PES spectra for different Cu concentrations in $Fe_{1-x}Cu_xCr_2S_4$ ($x = 0.1, 0.2, 0.5$), and found that they are very similar to each other, except for a small difference for the Cu 3d emission (see figure 7). Further, the valence-band spectra obtained at LT were also very similar to those obtained at RT. Therefore the RT valence-band PES spectra of $Fe_{0.5}Cu_{0.5}Cr_2S_4$ are shown in this paper as the representative valence-band PES spectra for $Fe_{1-x}Cu_xCr_2S_4$.

The top part of figure 5(a) shows the valence-band PES spectra of $Fe_{0.5}Cu_{0.5}Cr_2S_4$, obtained near the Cr $2p_{3/2}$ absorption edge. The labels (A–D) marked on the spectra denote the photon energies for which these PES spectra were obtained (see the arrows in figure 2). The sharp feature around 1.5 eV in binding energy (BE) is enhanced with increasing $h\nu$ from A to D, indicating it has mainly Cr 3d character due to the resonance effect in Cr $2p \rightarrow 3d$ RPES. The broader feature in the high BE side, which is marked and shifts away with increasing $h\nu$, is due to the Cr LMM Auger emission that occurs at a fixed kinetic energy (KE) of ∼572 eV. It has been observed that the T LMM Auger peaks reveal the resonant behaviour near the T $2p \rightarrow 3d$ RPES [38]. So it is necessary to separate out the direct Cr 3d PES peak from the overlapping Cr LMM Auger peak.

The procedure to extract the Cr 3d partial spectral weight (PSW) is shown in the bottom part of figure 5(a). Red and blue curves correspond to the on-resonance (D) and off-resonance (A) spectra, respectively, shown at the top. The curve at the bottom, marked with an arrow (brown) denotes the contribution of the Cr LMM Auger peak (from [39]), as marked in the top figure. The difference curve (open circles), which is obtained by subtracting both the off-resonance (A) spectrum and the Cr LMM Auger from the on-resonance spectrum (D), is considered to represent the Cr 3d PSW for $Fe_{0.5}Cu_{0.5}Cr_2S_4$. The extracted Cr 3d PSW exhibits a sharp peak around 1.5 eV in BE, shoulder-like features on the higher BE side, and negligible spectral intensity near E_F. Since Cr ions in $Fe_{1-x}Cu_xCr_2S_4$ are mainly trivalent ($3d^3$) (see figure 2), the absence of the Cr 3d states near E_F indicates that this sharp peak at ∼1.5 eV represents the $t_{2g}^3 \downarrow$ configuration of a Cr ion in $Fe_{1-x}Cu_xCr_2S_4$ (↓: majority spin).

Similarly, figure 5(b) shows the Fe $2p \rightarrow 3d$ RPES spectra of $Fe_{0.5}Cu_{0.5}Cr_2S_4$ and the extraction procedure for the Fe 3d PSW. All the notations are the same as in figure 5(a). The Fe LMM Auger emission occurs at KE ∼ 705 eV. This figure shows that the Fe 3d PSW is broad and structureless, which extends from E_F to ∼6 eV below E_F with the peak maximum around 4 eV. In contrast to the Cr 3d PSW (figure 5(a)), no sharp peaks are observed, suggesting that Fe 3d electrons are more itinerant than Cr 3d electrons. As will be discussed in figure 7, the Fe 3d PSW overlaps with the S 3p PSW quite a lot, indicating a large hybridization of Fe 3d states to S 3p states. The metallic-like bonding nature of Fe 3d electrons is quite different from the covalent and/or ionic bonding of Cr 3d and Cu 3d electrons. This conclusion is consistent with that of figure 4. Then the occupied Fe 3d electron configuration in $Fe_{1-x}Cu_xCr_2S_4$ will be $e_g^2 \uparrow t_{2g}^3 \uparrow e_g^y \downarrow (0 < y < 1)$.

Figure 6 presents the valence-band PES spectra of $Fe_{0.5}Cu_{0.5}Cr_2S_4$ over a wide $h\nu$ range (130 eV $\leqslant h\nu \leqslant$ 886 eV) and the Cr 3d and Fe 3d PSWs obtained in figure 5. The different line shapes with different $h\nu$ values are mainly due to the distinct contributions from different electronic states. This argument is supported by the $h\nu$ dependence of the relative strengths of the photoemission matrix elements of different electronic states. Since the photoemission matrix elements for $Fe_{0.5}Cu_{0.5}Cr_2S_4$ are not known, we have compared the calculated photoionization cross sections (σ_1 ($h\nu$)) of different orbitals as a function of $h\nu$ [40],

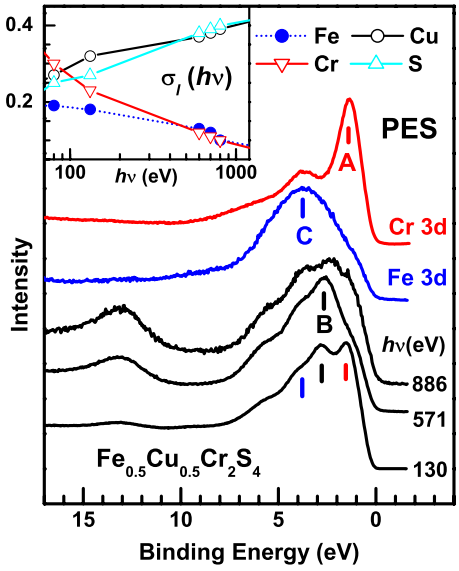

Figure 6. Comparison of the valence-band spectra of $Fe_{0.5}Cu_{0.5}Cr_2S_4$ over a wide $h\nu$ range (130 eV $\leqslant h\nu \leqslant$ 886 eV) and the Cr 3d and Fe 3d PSWs. Peak B has mainly Cu 3d character. Inset: relative ratio of the photoionization cross sections $\sigma_l(h\nu)$ of Fe 3d, Cu 3d, Cr 3d, and S 3p states.

as a first approximation (see the inset of figure 6). The inset plots the relative ratio of $\sigma_l(h\nu)$ values of Fe 3d, Cu 3d, Cr 3d, and S 3p states with respect to their sum ($\Sigma\sigma_l = 1$). In estimating $\sigma_l(h\nu)$ values, the number and the valence state of each ion per formula unit (fu) have been taken into account, and the calculated atomic photoionization cross sections have been used [40]. Then the cross section ratios of Fe 3d:Cu 3d:Cr 3d:S 3p in $Fe_{0.5}Cu_{0.5}Cr_2S_4$ are about 18%:32%:23%:27% at $h\nu \sim 130$ eV and about 13%:37%:12%:38% at $h\nu \sim 600$ eV. Note that the relative contribution from σ(Cr 3d) decreases rather fast from $h\nu \approx 130$ eV (23%) to $h\nu \approx 600$ eV (12%), resulting in the dominant Cu 3d and S 3p contributions for $h\nu >\sim 600$ eV. Therefore peak B (∼2.5 eV) at $h\nu = 571$ eV can be assigned to the Cu 3d states. Accordingly, peaks A (∼1.5 eV), B (∼2.5 eV), and C (∼4 eV) are identified to have the dominant Cr 3d, Cu 3d, and Fe 3d electron character, respectively. The assignment of the Cu 3d states will be discussed further in figure 7 based on the trend in the valence-band spectra with x. These assignments agree with those in the XES study [35] of $Fe_{1-x}Cu_xCr_2S_4$ for $x = 0$ and 0.5 and with the valence-band PES study [16] for $x = 0.5$.

Figure 7(a) compares the different PSWs for $Fe_{1-x}Cu_xCr_2S_4$. At $h\nu = 634$ eV, where the Cu 3d and S 3p electron emissions are much stronger than Fe 3d and Cr 3d emissions, peak B at ∼2.5 eV in BE increases with increasing Cu concentration (x), reflecting again that this ∼2.5 eV peak has mainly Cu 3d character. Figure 7(b) shows the schematic sketch of partial density of states (PDOS) of Fe 3d, Cu 3d, Cr 3d, and S 3p states in $Fe_{1-x}Cu_xCr_2S_4$. This schematic sketch is based on our experimental results, shown in figure 7(a). The Cr $t_{2g} \downarrow$ states are located at ∼1.5 eV below E_F, corresponding to the Cr^{3+} configuration ($t_{2g}^3 \downarrow$). The broad Fe $t_{2g}^3 \uparrow$ states extend from E_F to ∼6 eV below E_F, and the narrow Fe $e_g^2 \uparrow$ states are located around ∼4 eV below E_F. Since some of the Fe ions are divalent (Fe^{2+} ($e_g^2 \uparrow t_{2g}^3 \uparrow e_g^y \downarrow$) ($0 < y < 1$)), it is assumed that the Fe $e_g \downarrow$ states near E_F are split into two bands due to the local Jahn–Teller effect, one below E_F and the other above E_F, respectively. The nearly filled

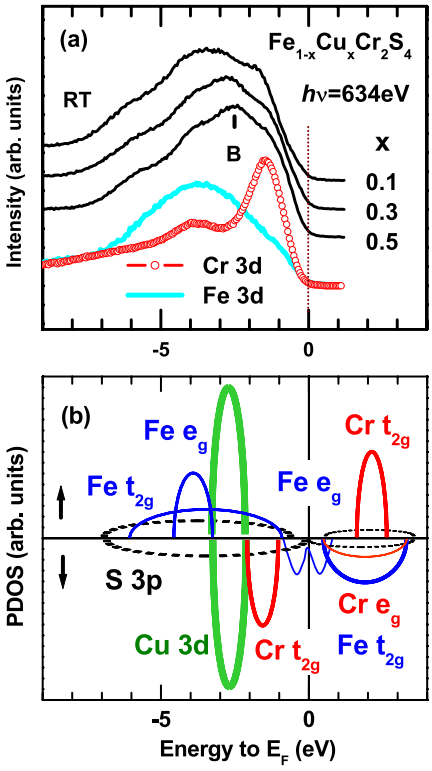

Figure 7. (a) Comparison of different PSWs for $Fe_{1-x}Cu_xCr_2S_4$. Peak B is assigned to the Cu 3d states. See the text for the details. (b) The schematic sketch of PDOS for $Fe_{1-x}Cu_xCr_2S_4$, based on the experiment.

Cu^+ 3d states ($3d^{10}$) are located around ∼2.5 eV below E_F. The S 3p states do not have sharp structures, and they are spread from E_F down to ∼6 eV below E_F. S 3p states overlap with all of the Fe 3d, Cu 3d, and Cr 3d states, reflecting the large hybridization to them, in particular to the Fe 3d states,

It is found that all of the Cr 3d, Fe 3d, and Cu 3d PSWs in $Fe_{1-x}Cu_xCr_2S_4$ ($x > 0$) have very small spectral intensity near E_F. Further, in contrast to the other two cations, the Fe 3d electrons seem to have metallic-like bonding character. These findings suggest that the topmost electronic states in the valence bands, i.e. those closest to E_F, have mainly the Fe 3d and S 3p character. This argument implies that the S 3p band is not fully occupied, and that the charge transfer may occur from the S ion to other sites in $Fe_{1-x}Cu_xCr_2S_4$. Differently from the case of oxide spinels, such charge transfer might be possible because of the smaller electron negativity of a S ion than an O ion. In this interpretation, $Fe_{1-x}Cu_xCr_2S_4$ can be classified as a kind of charge-transfer material, similarly as for $CuCr_2X_4$ (X = S, Se) [30].

The measured valence-band PES spectra of $Fe_{0.5}Cu_{0.5}Cr_2S_4$ do not show the metallic Fermi edge, but have the negligible spectral intensity near E_F, which is in agreement with our previous study [16]. The same features were observed for the samples with $0.1 \leqslant x \leqslant 0.5$. This observation suggests the very small density of states (DOS) at E_F in $Fe_{1-x}Cu_xCr_2S_4$. For studying the electronic structure very close to E_F, a high-resolution PES study on single-crystalline samples is required.

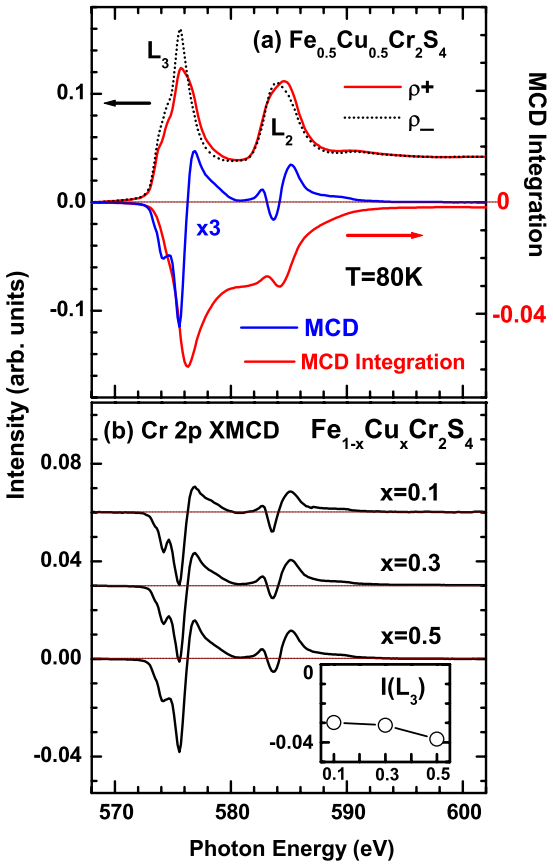

Figure 8. (a) The Cr 2p XAS spectra of $Fe_{0.5}Cu_{0.5}Cr_2S_4$, obtained with the photon helicity parallel to (ρ_+) and antiparallel to (ρ_-) to the magnetization, respectively. The XMCD spectrum (blue) corresponds to the difference between ρ_+ and ρ_- (XMCD $\equiv \rho_+ - \rho_-$). The bottom (red) line represents the integrated value of the XMCD spectrum. (b) Comparison of the Cr 2p XMCD spectra of $Fe_{1-x}Cu_xCr_2S_4$ ($x = 0.1, 0.3, 0.5$). They are on the same scale, but shifted vertically. Inset: plot of the intensity of the Cr L_3 XMCD peak versus x.

3.3. XMCD near T 2p absorption edges

In the following, we discuss the magnetic structure of $Fe_{1-x}Cu_xCr_2S_4$, by presenting the Cr and Fe 2p XMCD spectra in figures 8 and 9. These XMCD spectra were obtained at $T = 80$ K. Figure 8 shows the Cr 2p XMCD spectra of $Fe_{1-x}Cu_xCr_2S_4$. The top panel of figure 8(a) shows the XAS spectra of $Fe_{0.5}Cu_{0.5}Cr_2S_4$, obtained with the photon helicity parallel to (ρ_+) and antiparallel to (ρ_-) the magnetization, respectively. The bottom panel of figure 8(a) shows the Cr 2p XMCD ($\rho_+ - \rho_-$) spectrum (blue), which was obtained by taking the difference between ρ_+ and ρ_-, and the integrated value (red) of the XMCD spectrum ($\int(\rho_+ - \rho_-)$). The latter integration $\int(\rho_+ - \rho_-)$ can be used to estimate the spin magnetic moment (m_s) and the orbital magnetic moment (m_l) by applying the sum rule [24]. Figure 8(b) compares the Cr 2p XMCD spectra of $Fe_{1-x}Cu_xCr_2S_4$ for $x = 0.1$, 0.3, and 0.5. They are on the same scale, but shifted vertically. The inset of figure 8 plots the intensity of the Cr L_3 XMCD peak versus x, which is roughly proportional to m_s as a first approximation [41].

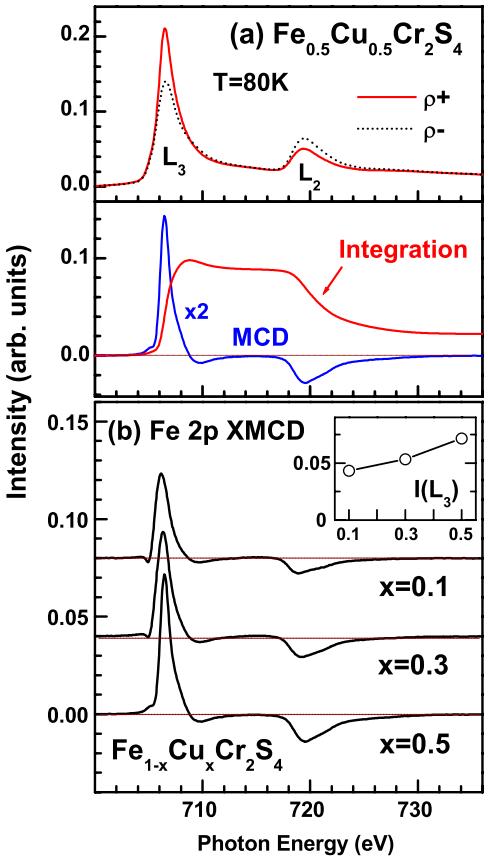

Figure 9. (a) Top: the Fe 2p XAS spectra of $Fe_{0.5}Cu_{0.5}Cr_2S_4$, obtained with the photon helicity parallel to (ρ_+) and antiparallel to (ρ_-) to the magnetization, respectively. (a) Bottom: the Fe 2p XMCD spectrum ($\rho_+ - \rho_-$: blue) and the integrated value (red) of the XMCD spectrum. (b) Comparison of the Fe 2p XMCD spectra of $Fe_{1-x}Cu_xCr_2S_4$ ($x = 0.1, 0.3, 0.5$). They are on the same scale, but shifted vertically. Inset: plot of the intensity of the Fe L_3 ($2p_{3/2}$) XMCD peak versus x.

Several observations are made in figure 8. First, the Cr 2p XMCD ($\rho_+ - \rho_-$) spectra of $Fe_{1-x}C_xCr_2S_4$ show the mostly negative and positive peaks around the L_3 and L_2 regions, respectively. Second, the Cr 2p XMCD spectra of $Fe_{1-x}C_xCr_2S_4$ are very similar to that of $CuCr_2X_4$ (X = S, Se) [30], indicating the large m_s on the Cr site. Third, the integrated XMCD over the whole range, $\int_{L_3+L_2}(\rho_+ - \rho_-)$, is very small, indicating that the orbital moment on the Cr ion is almost quenched. Finally, the relative intensity of the Cr L_3 XMCD signal (see the inset) increases with increasing x, indicating the increasing m_s on the Cr site.

Similarly, figure 9 shows the Fe 2p XMCD spectra of $Fe_{1-x}Cu_xCr_2S_4$ ($x = 0.1, 0.3, 0.5$). All the notations are the same as in figure 8. Several features have been observed in Fe 2p XMCD spectra of $Fe_{1-x}Cu_xCr_2S_4$ in figure 8: (i) The Fe 2p XMCD ($\rho_+ - \rho_-$) spectra show a mostly positive peak around the L_3 region but a mostly negative peak around the L_2 region. (ii) The Fe 2p XMCD spectra of $Fe_{1-x}Cu_xCr_2S_4$ are very similar to that of Fe metal [24], indicating that the electronic structure of the Fe 3d electrons in $Fe_{1-x}Cu_xCr_2S_4$ is metallic-like, and that there is large m_s on the Fe site in $Fe_{1-x}Cu_xCr_2S_4$. (iii) The relative intensity of the Fe L_3 XMCD signal increases with increasing x in $Fe_{1-x}Cu_xCr_2S_4$ (see the inset), indicating the

increasing m_s on the Fe site with increasing x. (iv) The polarity of the Fe 2p XMCD signals is opposite to that of the Cr 2p XMCD signals, implying the antiparallel alignment of the spin moments between Fe and Cr ions. (v) The integrated XMCD over the whole ($L_3 + L_2$) range, $\int_{L_3+L_2}(\rho_+ - \rho_-)$, with respect to that over the L_3 edge alone, $\int_{L_3}(\rho_+ - \rho_-)$, is larger than that in the Cr 2p XMCD. This observation indicates that the orbital moment on the Fe site is not completely quenched [24].

The trends in $I(L_3)$ for both Cr and Fe 2p XMCD spectra (see insets of figures 8 and 9) suggest that the magnitudes of the spin magnetic moments m_s of both Fe and Cr ions increase with increasing x in $Fe_{1-x}Cu_xCr_2S_4$ ($0.1 \leqslant x \leqslant 0.5$). The behaviour of the increasing m_s per Fe ion can be understood as follows. As discussed in figure 4, it is likely that there is a small increase in the Fe^{3+} (d^5) component with increasing x in $Fe_{1-x}Cu_xCr_2S_4$ even though the increasing valence states of Fe ions are not clearly observed in the Fe 2p XAS spectra due to the metallic-like character of Fe 3d electrons. Since the Fe^{3+} ion (d^5: $e_g^2 \uparrow t_{2g}^3 \uparrow$, $S = 5/2$) has a larger spin magnetic moment than the Fe^{2+} ion (d^6: $e_g^2 \uparrow t_{2g}^3 \uparrow e_g^1 \downarrow$, $S = 2$), the average spin magnetic moment per Fe ion will increase with increasing x. Note that, even if the spin magnetic moment per Fe ion increases, the total magnetic moment per fu of $Fe_{1-x}Cu_xCr_2S_4$ will still increase with increasing x [8, 42] because of the antiparallel alignment of the spin moments between Fe and Cr ions and the decreasing concentration of Fe ions. The origin of the increasing magnetic moment per Cr ion with increasing x is not well understood at the moment.

4. Conclusions

We have determined the valence states of all three constituent transition-metal elements in $Fe_{1-x}Cu_xCr_2S_4$ ($0.1 \leqslant x \leqslant 0.5$) by employing T 2p XAS and T 2p $\rightarrow$ 3d RPES. The measured T 2p XAS spectra (T = Cr, Cu) show that Cu ions are nearly monovalent (+), that Cr ions are nearly trivalent (3+), and that the valence states of Cr and Cu ions do not change with x. This finding is consistent with the model by Lotgering *et al* rather than that by Goodenough. The measured Fe 2p XAS spectra are very similar to that of Fe metal, indicating the metallic-like bonding due to the large hybridization between the Fe 3d and S 3p states. The Fe and Cr 2p XMCD measurements show that the magnetic moments of Cr ions and Fe ions are aligned antiparallel to each other, and that both the Cr and Fe magnetic moments increase with increasing x. The increasing spin magnetic moment per Fe ion with increasing x in $Fe_{1-x}Cu_xCr_2S_4$ can be understood as due to a small increase in the Fe^{3+} component, as compared to the Fe^{2+} component. The analysis of the Cr 2p XMCD spectra reveals that the orbital moment on the Cr ion is almost quenched.

By combining the Cr and Fe 2p $\rightarrow$ 3d RPES and the $h\nu$-dependences of the different valence-band features in $Fe_{1-x}Cu_xCr_2S_4$, the Fe 3d, Cr 3d, Cu 3d, and S 3p PSWs have been determined. The measured valence-band PES data suggest that the Cr $t_{2g} \downarrow$ states are located at $\sim$1.5 eV below E_F, corresponding to the Cr^{3+} configuration ($t_{2g}^3 \downarrow$). Our PES study also reveals that the Fe $t_{2g}^3 \uparrow$ states are rather broad, extending from E_F to $\sim$6 eV below E_F, that the Fe $e_g^2 \uparrow$ states are located around $\sim$4 eV below E_F, and that the Fe $e_g \downarrow$ states are located very close to E_F. The Cu 3d orbitals are nearly filled ($3d^{10}$) and located around $\sim$2.5 eV below E_F. The S 3p states do not have sharp structures, and they are spread from E_F down to $\sim$6 eV below E_F. This study suggests that the charge transfer occurs from Fe and S ions to other ions for $x > 0$, producing holes in the S 3p–Fe 3d hybridized bands. Our findings suggest that the narrow hybridized Fe $e_g \downarrow$–S 3p states near E_F play an important role in determining the transport properties in $Fe_{1-x}Cu_xCr_2S_4$ for $x \leqslant 0.5$.

Acknowledgments

This work was supported by the KRF (KRF-2005-204-C00023), by the KOSEF through the CSCMR at SNU and the eSSC at POSTECH, and in part by the 2006 Research Fund of the Catholic University of Korea. The PAL is supported by the MOST and POSCO in Korea.

References

[1] Watanabe T and Nakada I 1978 *Japan. J. Appl. Phys.* **17** 1745
[2] Ramirez A P, Cava R J and Krajewski J 1997 *Nature* **386** 156
[3] Kim S J, Son B S, Lee B W and Kim C S 2004 *J. Appl. Phys.* **95** 6837
[4] Haacke G and Beegle L C 1967 *J. Phys. Chem. Solids* **28** 1699
[5] Lotgering F K, van Stapele R P, van der Steen G H A M and van Wieringen J S 1969 *J. Phys. Chem. Solids* **30** 799
[6] Ando K, Nishihara Y, Okuda T and Tsushima T 1979 *J. Appl. Phys.* **50** 1917
[7] Fritsch V *et al* 2003 *Phys. Rev.* B **67** 144419
[8] Park M S, Kwon S K, Youn S J and Min B I 1999 *Phys. Rev.* B **59** 10018
[9] Lotgering F K and van Stapele R P 1967 *Solid State Commun.* **5** 143
[10] Goodenough J B 1969 *J. Phys. Chem. Solids* **30** 26
[11] Lu Z W *et al* 1996 *Phys. Rev.* B **53** 9626
[12] Matsuno J, Mizokawa T, Fujimori A, Zatsepin D A, Galakhov V R, Kurmaev E Z, Kato Y and Nagata S 1997 *Phys. Rev.* B **55** R15979
[13] Hart G L W, Pickett W E, Kurmaev E Z, Hartmann D, Neumann M, Moewes A, Ederer D L, Endoh R, Taniguchi K and Nagata S 2000 *Phys. Rev.* B **61** 4230
[14] Colominas C 1967 *Phys. Rev.* **153** 558
[15] Tsurkan V, Demeter M, Schneider B, Hartmann D and Neumann M 2000 *Solid State Commun.* **114** 149
[16] Kang J-S, Kim S J, Kim C S, Olson C G and Min B I 2001 *Phys. Rev.* B **63** 144412
[17] Locher P R 1967 *Solid State Commun.* **5** 185
[18] Krok-Kowalski J, Gron T, Warczewski J, Mydlarz T and Okonska-Kozlowska I 1997 *J. Magn. Magn. Mater.* **168** 129
[19] Chen Z, Tan S, Yang Z and Zhang Y 1999 *Phys. Rev.* B **59** 11172
[20] Hüfner S 1995 Photoelectron spectroscopy *Solid-State Sciences* vol 82 (Berlin: Springer)
[21] de Groot F M F, Fuggle J C, Thole B T and Sawatzky G A 1990 *Phys. Rev.* B **42** 5459
[22] van der Laan G and Kirkman I W 1992 *J. Phys.: Condens. Matter* **4** 4189
[23] Thole B T, Carra P, Sette F and van der Laan G 1992 *Phys. Rev. Lett.* **68** 1943
[24] Chen C T, Idzerda Y U, Lin H-J, Smith N V, Meigs G, Chaban E, Ho G H, Pellegrin E and Sette F 1995 *Phys. Rev. Lett.* **75** 152
[25] Regan T J, Ohldag H, Stamm C, Nolting F, Lüning J, Stöhr J and White R L 2001 *Phys. Rev.* B **64** 214422
[26] Kang J-S *et al* 2005 *Phys. Rev. Lett.* **94** 147202
[27] Theil C, van Elp J and Folkmann F 1999 *Phys. Rev.* B **59** 7931
[28] Kurmaev E Z, Moewes A, Butorin S M, Katsnelson M I, Finkelstein L D, Nordgren J and Tedrow P M 2003 *Phys. Rev.* B **67** 155105
[29] Huang D J *et al* 2002 *Phys. Rev.* B **66** 174440
[30] Kimura A, Matsuno J, Okabayashi J, Fujimori A, Shishidou T, Kulatov E and Kanomata T 2001 *Phys. Rev.* B **63** 224420
[31] Tomaz M A, Antel W J, O'Brien W L and Harp G R 1997 *Phys. Rev.* B **55** 3716
[32] Chang C F, Huang D J, Tanaka A, Guo G Y, Chung S C, Kao S-T, Shyu S G and Chen C T 2005 *Phys. Rev.* B **71** 052407
[33] van der Laan G, Pattrick R A D, Charnock J M and Grguric B A 2002 *Phys. Rev.* B **66** 045104
[34] Finazzi M, Ghiringhelli G, Tjernberg O, Ohresser Ph and Brookes N B 2000 *Phys. Rev.* B **61** 4629
[35] Kurmaev E Z *et al* 2000 *J. Phys.: Condens. Matter* **12** 5411
[36] Deb A, Mizumaki M, Muro T, Sakurai Y and Tsurkan V 2003 *Phys. Rev.* B **68** 014427
[37] Dietl T 2002 *Semicond. Sci. Technol.* **17** 377
[38] Kang J-S *et al* 2003 *Phys. Rev.* B **68** 012410
[39] Herdberg C L (ed) 1995 *Handbook of Auger Electron Spectroscopy* 3rd edn (Minnesota: Physical Electronics)
[40] Yeh J J and Lindau I 1985 *At. Data Nucl. Data Tables* **32** 1 where calculated atomic photoionization cross sections are given
[41] Wu R and Freeman A J 1994 *Phys. Rev. Lett.* **73** 1994
[42] Son S B, Kim S J, Lee B W and Kim C S 2005 *J. Magn. Magn. Mater.* **290/291** 381